

UTX/KDM6A Deletion Promotes Recovery of Spinal Cord Injury by Epigenetically Regulating Vascular Regeneration

Shuangfei Ni,^{1,3,4,7} Zixiang Luo,^{1,3,4,7} Liyuan Jiang,^{1,3,4} Zhu Guo,^{1,3,4,5} Ping Li,^{1,3,4} Xiang Xu,^{1,3,4,6} Yong Cao,^{1,3,4} Chunyue Duan,^{1,3,4} Tianding Wu,^{1,3,4} Chengjun Li,^{1,3,4} Hongbin Lu,^{2,3,4} and Jianzhong Hu^{1,3,4}

¹Department of Spine Surgery, Xiangya Hospital, Central South University, 410008 Changsha, China; ²Department of Sports Medicine, Xiangya Hospital, Central South University, 410008 Changsha, China; ³Key Laboratory of Organ Injury, Aging and Regenerative Medicine of Hunan Province, 410008 Changsha, China; ⁴Research Centre of Sports Medicine, Xiangya Hospital, Central South University, 410008 Changsha, China; ⁵Spine Surgery Department of the Affiliated Hospital of Qingdao University, 266000 Qingdao, China; ⁶Department of Minimally Invasive Spinal Surgery, The Second Affiliated Hospital of Inner Mongolia Medical College, Huhhot 010030, Inner Mongolia, China

The regeneration of the blood vessel system post spinal cord injury (SCI) is essential for the repair of neurological function. As a significant means to regulate gene expression, epigenetic regulation of angiogenesis in SCI is still largely unknown. Here, we found that Ubiquitously Transcribed tetratricopeptide repeat on chromosome X (UTX), the histone H3K27 demethylase, increased significantly in endothelial cells post SCI. Knockdown of UTX can promote the migration and tube formation of endothelial cells. The specific knockout of UTX in endothelial cells enhanced angiogenesis post SCI accompanied with improved neurological function. In addition, we found regulation of UTX expression can change the level of microRNA 24 (miR-24) *in vitro*. The physical binding of UTX to the promotor of miR-24 was indicated by chromatin immunoprecipitation (ChIP) assay. Meanwhile, methylation sequencing of endothelial cells demonstrated that UTX could significantly decrease the level of methylation in the miR-24 promotor. Furthermore, miR-24 significantly abolished the promoting effect of UTX deletion on angiogenesis *in vitro* and *in vivo*. Finally, we predicted the potential target mRNAs of miR-24 related to angiogenesis. We indicate that UTX deletion can epigenetically promote the vascular regeneration and functional recovery post SCI by forming a regulatory network with miR-24.

INTRODUCTION

Spinal cord injury (SCI) is a devastating event with high morbidity and mortality throughout the world. As the epidemiological data showed in 2018, the global incidence of traumatic SCI was 10.5 cases per 100,000 persons. In other words, there are an estimated 768,473 new cases annually worldwide.¹

Acute disruption of the microvasculature structure occurs immediately and results in the breakdown of the blood-spinal cord barrier (BSCB), death of endothelial cell (EC), and increase of vascular permeability when primary SCI happens.² These comprehensive vascular damages trigger a cascade of secondary pathological processes including inflam-

mation and glial and fibrotic scar formation to prevent tissue regeneration and functional recovery furthermore.^{3,4} As an important structure to steadily supply nutrients and oxygen, microvessels occupy a crucial role in neurogenesis and maintenance of physiological function.⁵ After SCI, the lack of vascular networks aggravated ischemia and apoptosis of neural tissue in the epicenter of the spinal cord.² Angiogenesis, in which the newly formed microvessels arise via sprouting from pre-existing vessels or proliferation in the injury core,⁶ is considered a manifestation of tissue repair.² Hence, targeting angiogenesis at the early stage of SCI can reduce the amount of cell loss and neurological deficits. Moreover, neural tissue repair and function recovery, especially with the chronicity of SCI, would be improved.⁷

Epigenetic modifications are defined as reversible processes involving the change of cells' DNA or histones that affect gene expression without altering the DNA sequence.⁸ It includes DNA methylation, histone modification, non-coding RNA, and chromosomal conformation, which play an essential role in the development and physiological and pathological events of organisms, and contribute to the regulation of cell fate, the maintenance of cell specificity, and cell-type-specific functions.^{9,10} Methylation of histone H3 lysine (K) residue 27 (H3K27) in the promoters of genes was identified as a sign of repression, whereas demethylation of H3K27me3 did the opposite function.¹¹ Several studies demonstrated that the abilities of blood vessel formation, angiogenic properties (capillary-like structure formation), EC adhesion, and migration were closely related to the methylation state of the H3K27 locus.¹²⁻¹⁶ The Ubiquitously

Received 25 April 2019; accepted 12 August 2019;
<https://doi.org/10.1016/j.ymthe.2019.08.009>.

⁷These authors contributed equally to this work.

Correspondence: Hongbin Lu, Department of Sports Medicine, Xiangya Hospital, Central South University, 410008 Changsha, China.

E-mail: hongbinlu@hotmail.com

Correspondence: Jianzhong Hu, Department of Spine Surgery, Xiangya Hospital, Central South University, 410008 Changsha, China.

E-mail: jianzhonghu@hotmail.com



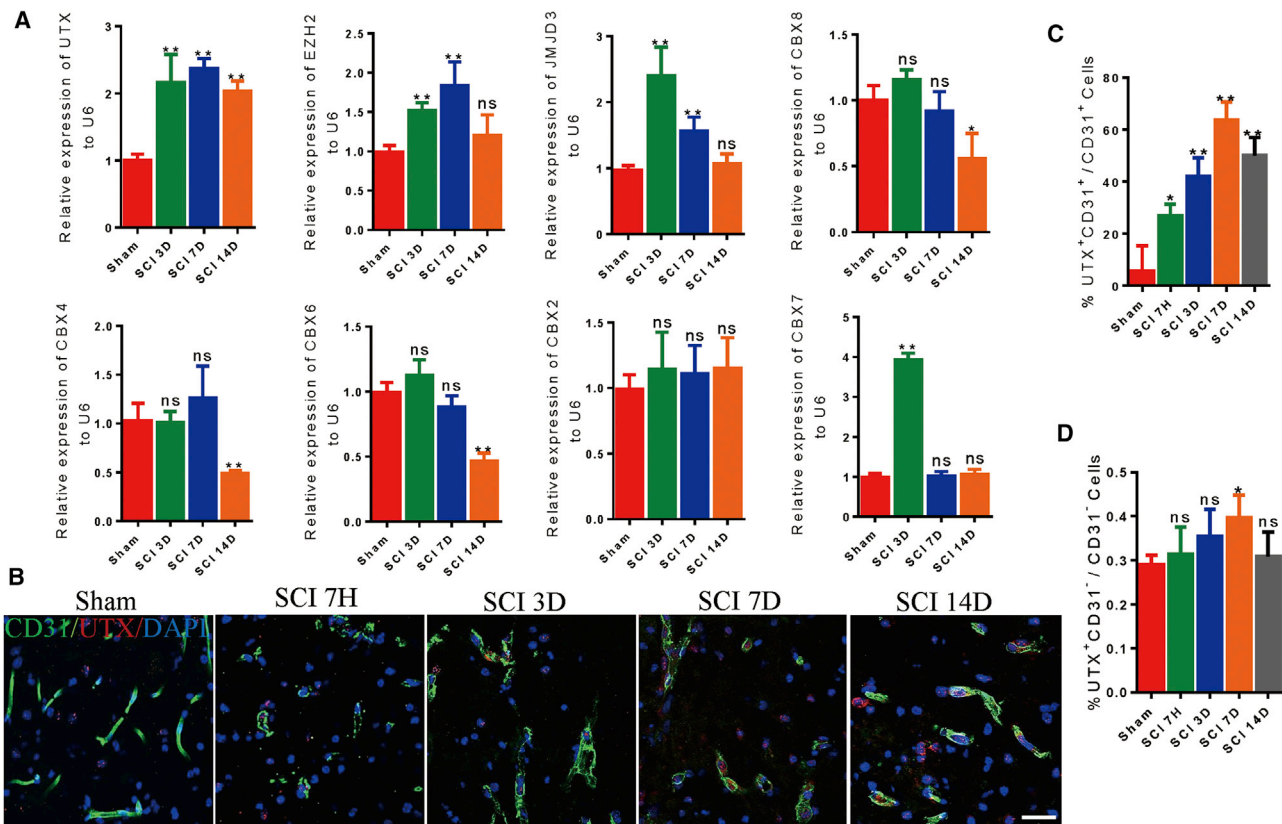


Figure 1. Increase of UTX in Endothelial Cells of the Spinal Cord Post SCI

(A) The changes of several key epigenetic regulators at 3, 7, and 14 days post SCI by qRT-PCR, including UTX, EZH2, JMJD3, CBX8, CBX4, CBX6, CBX2, and CBX7. $n = 5$ per group. (B) Representative images of spinal cord sections stained for UTX (red) and CD31 (green) in the sham group and at 7 h, 3 days, 7 days, and 14 days post SCI. Scale bar, 50 μm . (C) Percentage of UTX⁺CD31⁺ cells in CD31⁺ cells. (D) Percentage of UTX⁺CD31⁻ cells in CD31⁻ cells. Bars indicate mean \pm SEM; $n = 6$ per group. * $p < 0.05$, ** $p < 0.01$ compared with sham surgery group. ns, no significance.

Transcribed tetratricopeptide repeat on chromosome X (UTX)/Lysine Demethylase 6A (KDM6A) is a histone demethylase enzyme responsible for removing the methyl group of H3K27me3/H3K27me2 to initiate the transcription of target genes.^{17,18} However, the molecular mechanisms underlying UTX regulation in the process of angiogenesis have not been fully elucidated.

MicroRNAs (miRNAs), known as non-protein-coding nucleotide RNAs, can negatively regulate the expression of target mRNAs at the posttranscriptional level.¹⁹ To date, several miRNAs have been detected in the nervous system to regulate various pathophysiological processes.²⁰ The repair of impaired endothelial functions was also regulated by a series of miRNAs.^{21–23} MicroRNA 24 (miR-24) was a widely expressed molecule in a variety of organs, especially enriched in ECs.²⁴ It involved in the course of ECs apoptosis, necrosis, proliferation, and pro-angiogenesis, whereas the role in SCI remains basically uncertain.^{25–27}

In the present study, we report that the expression of UTX increases post SCI. The knockout (KO) of UTX in ECs can promote the

vascular regeneration post SCI by regulating the promoter hypermethylation of miR-24.

RESULTS

The Expression of UTX Increased in ECs of the Spinal Cord Post SCI in Mice

To demonstrate the potential role of epigenetic regulators in SCI (thoracic vertebra level 10 [T10] contusive in mice, moderate), we examined by qRT-PCR the changes of several key epigenetic regulators in the spinal cord (1 cm around injury site) post SCI. We found that the mRNA level of UTX, EZH2, JMJD3, CBX8, CBX4, CBX6, and CBX7 changed significantly at different time points post SCI (Figure 1A). Among them, only UTX increased significantly at 3 days and remained high at 7 and 14 days post SCI (Figure 1A). More importantly, the immunofluorescent staining of spinal cord sections further demonstrated that the increase of UTX mainly occurred in CD31⁺ ECs post SCI (Figures 1B and 1C), although the expression of UTX also slightly increased in CD31⁻ cells post SCI (Figure 1D). Together, these results imply the potential function of UTX in vascular regeneration post SCI.

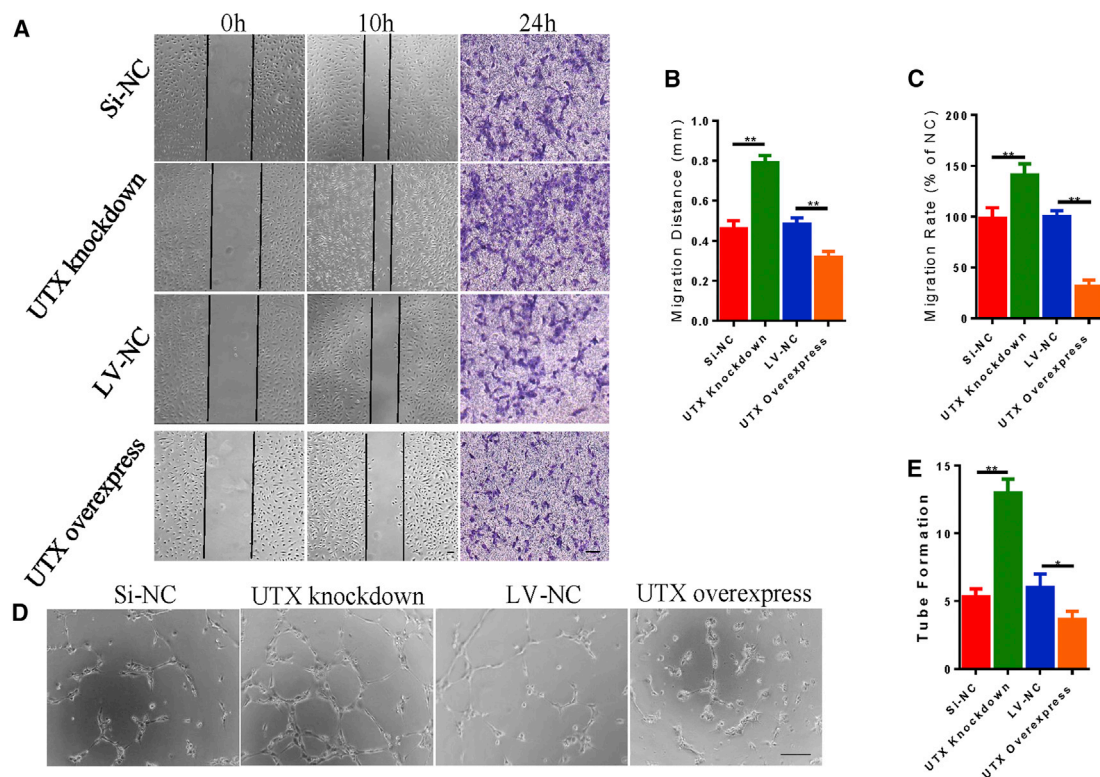


Figure 2. Effect of UTX on Migration and Tube Formation of Endothelial Cells *In Vitro*

(A) Representative images of horizontal migration by wound healing experiment (first and second columns) and vertical migration by Transwell experiment (third column) of HUVECs in the Si-NC group, UTX knockdown group, LV-NC group, and UTX overexpression group. Scale bars, 100 μ m. (B and C) Quantification of (A): migration distance (B) and migration rate (C). (D) Representative images of canaliculation of HUVECs in the Si-NC group, UTX knockdown group, LV-NC group, and UTX overexpression group. Scale bar, 200 μ m. (E) Quantification of (D). Bars indicate mean \pm SEM; $n = 6$ per group. * $p < 0.05$, ** $p < 0.01$ compared with the control group. LV-NC, empty vector for negative control; Si-NC, scramble for negative control; UTX overexpression, lentivirus for UTX overexpression; UTX knockdown, siRNA for UTX knockdown.

The Effect of UTX on Migration and Tube Formation of ECs *In Vitro*

To further explore the potential effect of UTX on ECs, we conducted the knockdown and upregulation of UTX in human umbilical vein ECs (HUVECs). The regulative efficiency of UTX expression was validated by western blot (Figures S1A and S1B). Immunostaining demonstrated that knockdown of UTX significantly promoted the horizontal and vertical migration of HUVECs, as indicated by wound healing and Transwell experiments (Figures 2A–2C), whereas the upregulation of UTX significantly inhibited the horizontal and vertical migration of HUVECs (Figures 2A–2C). Furthermore, the canaliculation of HUVECs *in vitro* was significantly promoted by UTX knockdown and reduced by UTX upregulation, as indicated by the number of tube formations (Figures 2D and 2E).

UTX KO in Tek⁺ ECs Promoted Vascular Regeneration and Functional Recovery Post SCI

To elucidate the role of UTX in vascular regeneration post SCI, we knocked out UTX specifically in Tek⁺ ECs by crossbreeding Tek-Cre mice with UTX floxed mice (Tek^{Cre}; UTX^{lox/lox}, named “UTX^{-/-} mice”). Immunostaining of spinal cord sections demon-

strated that the CD31⁺ area significantly increased at 7, 14, and 28 days post SCI in UTX^{-/-} mice compared with their age-matched wild-type (WT) littermates (herein called UTX^{+/+} mice) (Figures 3A and 3B), indicating the increased vascular regeneration in UTX^{-/-} mice post SCI. In parallel, the three-dimensional microvasculature of the spinal cord was visualized by Synchrotron radiation micro-tomography (SR μ CT) in UTX^{-/-} mice and UTX^{+/+} mice at 28 days post sham or SCI surgery (Figure 3C), the theoretical spatial resolution of which is as high as 3.25 μ m/pixel. The quantitative analysis demonstrated that the functional vascular regeneration of injured spinal cord in UTX^{-/-} mice was significantly higher than that in UTX^{+/+} mice, as indicated by the vessel volume fraction (Figure 3D). Then, several behavior tests were conducted to evaluate the functional recovery in UTX^{-/-} mice. First, the withdraw thresholds responding to mechanical stimuli and heat stimuli decreased significantly in UTX^{-/-} mice over time post SCI compared with their age-matched UTX^{+/+} mice (Figures 3E and 3F), indicating the sensory improvement in UTX^{-/-} mice post SCI. Then, the locomotive evaluation demonstrated that the Basso mouse scale (BMS) scores of UTX^{-/-} mice were significantly higher than those of UTX^{+/+} mice over time post SCI (Figure 3G), indicating the improved locomotive function in

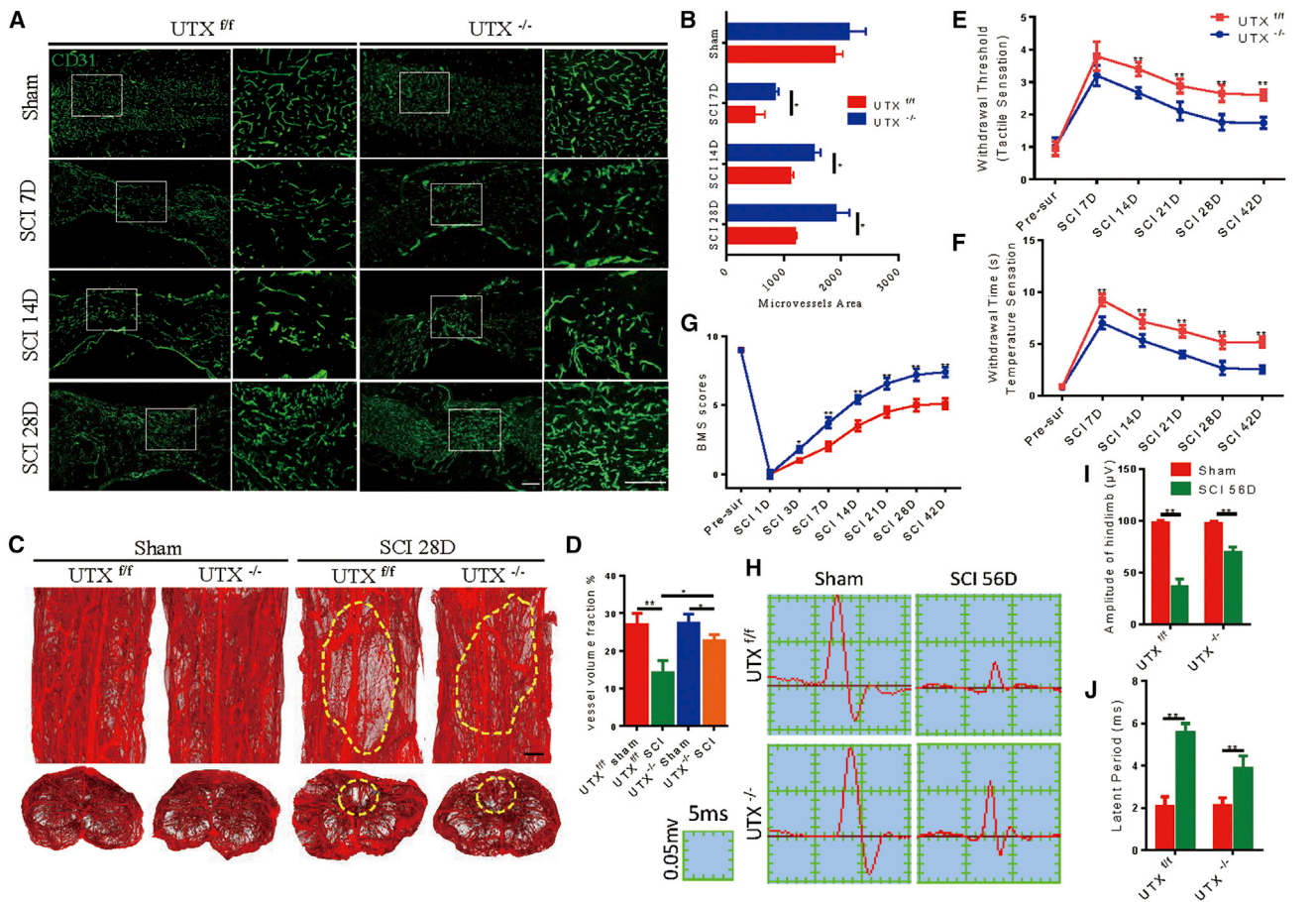


Figure 3. UTX KO in Tek⁺ Endothelial Cells Promoted Vascular Regeneration and Functional Recovery Post SCI

(A) Representative images of immunofluorescent analysis of CD31⁺ (green) blood vessels in the mouse spinal cord at 7, 14, and 28 days post SCI in UTX^{-/-} and UTX^{f/f} mice. Scale bars, 100 μm. (B) Quantification of (A). (C) The three-dimensional microvasculature of the spinal cord at T10 level in UTX^{f/f} and UTX^{-/-} mice at 28 days post sham or SCI surgery. Scale bar, 100 μm. (D) Quantification of the vessel volume fraction of (C). (E) The hind paw withdrawal threshold responding to mechanical stimulation over time post SCI in UTX^{-/-} and UTX^{f/f} mice. (F) The hind paw withdrawal time responding to heat stimulation over time post SCI in UTX^{-/-} and UTX^{f/f} mice. (G) BMS scores over time post SCI in UTX^{-/-} and UTX^{f/f} mice. (H) Representative images of motor-evoked potential (MEP) at 56 days post SCI in UTX^{-/-} and UTX^{f/f} mice. (I) Quantification of the amplitude of MEP in (H). (J) Quantification of the latent period of MEP in (H). Bars indicate mean ± SEM; n = 6 per group. *p < 0.05, **p < 0.01 compared with sham group or pre-surgery.

UTX^{-/-} mice post SCI. Moreover, the electrophysiological analysis demonstrated that the amplitude of motor-evoked potentials (MEPs) increased significantly, and the latent period decreased significantly in UTX^{-/-} mice compared with UTX^{f/f} mice at 56 days post SCI (Figures 3H–3J), validating the functional recovery of UTX^{-/-} mice. Taken together, these findings implied that UTX KO in ECs can promote vascular regeneration and improve the sensory and locomotive function post SCI.

UTX Directly Binds to and Demethylates the Promotor of miR-24 in ECs

Previously, we showed that miR-24 is one of the most differentially expressed miRNAs in the spinal cord post SCI by microarray analysis. Here, *in situ* hybridization of miR-24 further demonstrated the increased expression of miR-24 in CD31⁺ ECs at 14 days post SCI (Figure S2). Then, we found that the overexpression of UTX signifi-

cantly increased the level of miR-24 in HUVECs, whereas the knock-down of UTX significantly decreased the level of miR-24, as indicated by qRT-PCR (Figures 4A and 4B). To further determine the mechanism by which UTX regulates the expression of miR-24, we performed the chromatin immunoprecipitation (ChIP) assay to detect the potential binding site of UTX on the miR-24 promoter. ChIP assay revealed that UTX can specifically bind to the promoter of miR-24 in HUVECs (Figures 4C–4E; Figure S5), indicating that UTX and miR-24 form an epigenetic regulative complex. Importantly, the effect of UTX on the methylation level of CpG position (No. 1–17) in the miR-24 promoter was analyzed, showing that UTX can significantly decrease the methylation level of several CpG positions (No. 1, 7, and 9) in the miR-24 promoter (Figures 4F and 4G). Moreover, the total unmethylation level was significantly higher in the UTX overexpression group compared with the negative control group (Figure 4H). Taken together, UTX can directly bind to the

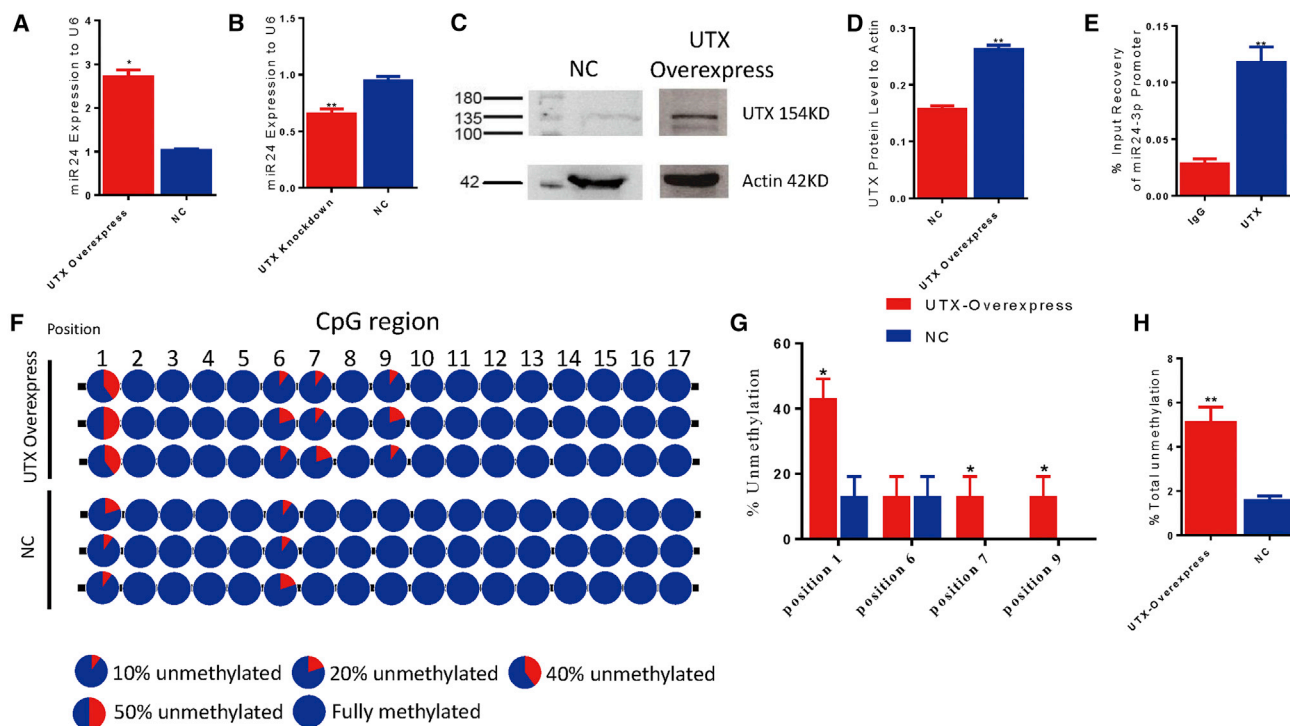


Figure 4. UTX Directly Binds to and Demethylates the Promotor of miR-24

(A) qRT-PCR analysis of miR-24 in HUVECs of the UTX overexpression group and control group. (B) qRT-PCR analysis of miR-24 in HUVECs of the UTX knockdown group and control group. * $p < 0.05$, ** $p < 0.01$ compared with the sham group. $n = 6$ per group. (C) Western blot analysis of UTX and actin in the product of chromatin immunoprecipitation, showing the band of UTX at 154 kDa. (D) Quantification of (C). ** $p < 0.01$ compared with the control group. $n = 3$ per group. (E) The level of miR-24 promoter in the product of chromatin immunoprecipitation in the UTX pull-down group and IgG pull-down group. ** $p < 0.01$ compared with the IgG group. $n = 3$ per group. (F) The methylation level of the CpG region in the miR-24 promoter in the UTX overexpression group and control group. (G) Quantification of the unmethylation level of positions 1, 6, 7, and 9 in the CpG region. * $p < 0.05$ compared with the control group at the corresponding position. $n = 3$ per group. (H) Quantification of the total unmethylation level in the CpG region. Bars indicate mean \pm SEM; $n = 3$ per group. ** $p < 0.01$ compared with the control group.

promotor of miR-24 to decrease the methylation level and then promote the expression of miR-24.

miR-24 Abolished the Effect of UTX Knockdown on Migration and Canaliculation of ECs

To determine the effect of miR-24 on the function of ECs, we regulated the expression of miR-24 *in vitro*. The regulative efficiency of miR-24 expression was validated by qRT-PCR (Figure S3A). We found that overexpression of miR-24 significantly repressed the horizontal and vertical migration of HUVECs, whereas knockdown of miR-24 significantly promoted the migration of HUVECs, as indicated by wound healing and Transwell experiments (Figures 5A–5C). In parallel, upregulation of miR-24 significantly repressed the canaliculation of HUVECs, whereas knockdown of miR-24 significantly promoted the canaliculation of HUVECs, determined by the number of tube formations (Figures 5D and 5E). These findings indicate that miR-24 inhibits the migration and canaliculation of ECs *in vitro*, similar to that of UTX *in vitro*.

To validate whether UTX functionalized through regulation of miR-24, we conducted the co-modification of UTX and miR-24 to

simultaneously knock down UTX and upregulate miR-24 in HUVECs. The regulative efficiency of miR-24 expression was validated by qRT-PCR (Figure S3B). Wound healing and Transwell experiments demonstrated that upregulation of miR-24 significantly abolished the positive effect of UTX knockdown on the horizontal and vertical migration of HUVECs (Figures 6A–6C) and canaliculation of HUVECs (Figures 6D and 6E). Together, knockdown of UTX promotes the migration and canaliculation by potentially repressing miR-24 expression.

miR-24 Inhibited Vascular Regeneration in UTX^{-/-} Mice Post SCI

To further determine whether UTX KO promoted vascular regeneration post SCI by regulating miR-24, we upregulated the expression of miR-24 in the spinal cord by injection of lentivirus-miR-24 immediately post SCI. The efficiency of miR-24 overexpression was validated by *in situ* hybridization of miR-24 and qRT-PCR (Figures S4A–S4D). Immunofluorescent staining of spinal cord sections demonstrated that the CD31⁺ area significantly increased in injury site at 28 days post SCI in UTX^{-/-} mice compared with their age-matched UTX^{+/+} littermates (Figures 7A and 7B). Notably, the CD31⁺ area decreased significantly in injury site at 28 days post SCI in UTX^{-/-} mice with

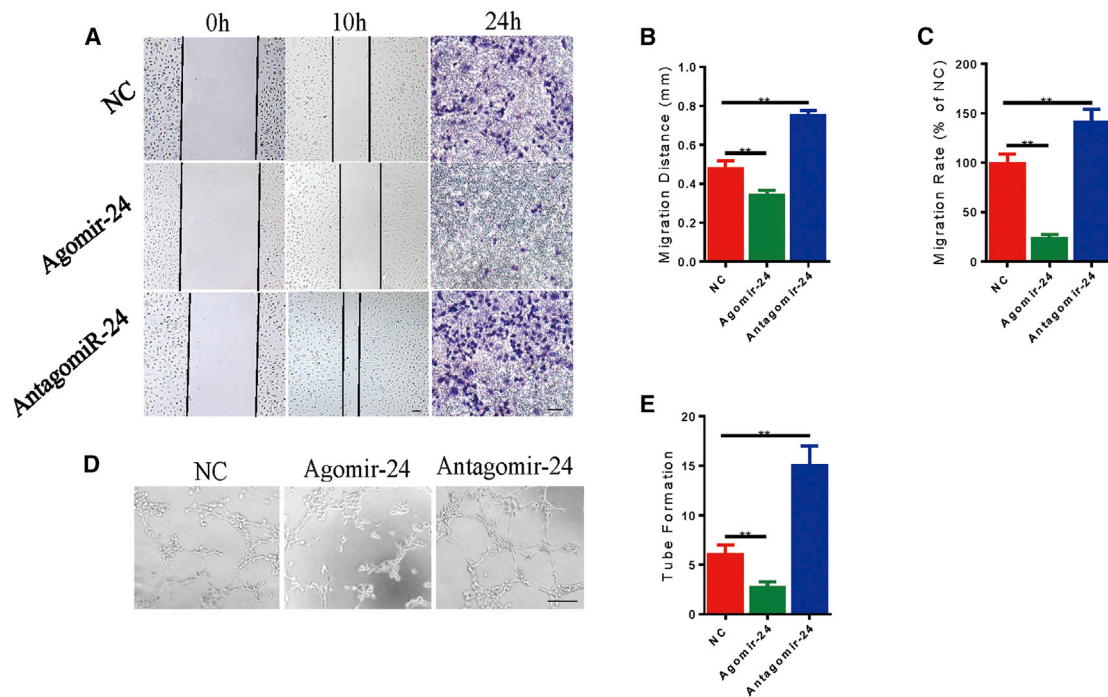


Figure 5. Inhibition of miR-24 Benefited the Migration and Tube Formation of Endothelial Cells *In Vitro*

(A) Representative images of horizontal migration by wound healing experiment (first and second columns) and vertical migration by Transwell experiment (third column) of HUVECs in the miR-24 knockdown group, miR-24 overexpression group, and control group. Scale bars, 100 μ m. (B and C) Quantification of (A): migration distance (B) and migration rate (C). (D) Representative images of canalicularization of HUVECs in the miR-24 knockdown group, miR-24 overexpression group, and control group. Scale bar, 200 μ m. (E) Quantification of (D). Bars indicate mean \pm SEM; n = 6 per group. **p < 0.01 compared with the control group.

miR-24 overexpression compared with UTX^{-/-} mice, indicating that miR-24 obstructs the vascular regeneration in the injury site in UTX^{-/-} mice at 28 days post SCI (Figures 7A and 7B). The electrophysiological analysis demonstrated that the amplitude of MEP increased and the latent period decreased significantly in UTX^{-/-} mice compared with UTX^{+/+} mice at 56 days post SCI (Figures 7C–7E). However, the overexpression of miR-24 in UTX^{-/-} mice significantly reduced the amplitude and prolonged the latent period of MEP compared with UTX^{-/-} mice at 56 days post SCI (Figures 7C–7E).

Prediction of miR-24 Target Genes

In order to identify miR-24-targeted genes involved in vascular regeneration, we first searched the AmiGO 2 website of gene ontology (<http://amigo.geneontology.org/amigo>) and found that 514 mouse genes are potentially related to angiogenesis. Then, bioinformatics miRNA targets prediction tools (<http://www.targetscan.org>; <http://mirdb.org>) were used to identify potential miR-24 targets. As the Venn diagram displayed (Figure 8A), there are 654 mouse genes with putative 3' UTR binding sites for miR-24 retrieved in TargetScan and 966 mouse genes retrieved in miRDB. Finally, the Venn diagram showed that in total 21 mouse genes encompassed potential functions in endothelial angiogenesis (Figure 8A; Table S1). In parallel, we also predicted that there were 24 potential miR-24 target genes associated with angiogenesis in humans (Figure 8B; Table S1). In the predicted

genes, 15 genes are the same for mouse and human (Table S1). Among them, FZD5, PAK4, MAPK7, and S1PR1 have been validated as the target genes of miR-24.^{24,28–30} We examined the changes of these genes in the spinal cord (1 cm around injury site) post SCI in UTX^{+/+} and UTX^{-/-} mice by qRT-PCR. We found that the mRNA levels of FZD5, PAK4, and MAPK7 were significantly higher in UTX^{-/-} mice than that in UTX^{+/+} mice at 7 days post SCI (Figure 8C).

DISCUSSION

Acute SCI is a catastrophic trauma that initiates the changes of multiple intrinsic genes, which is a major obstacle for functional recovery after SCI.³¹ As a key mechanism mediating gene transcription, epigenetics plays a critical role in the pathological changes of traumatic diseases.³² However, far too few studies have focused on SCI. Additionally, previous studies are mainly neurocentrically focused, which is considered insufficient as the emerging concept of the neurovascular unit.^{33–36} Our previous studies demonstrated that targeting vascular regeneration was a potential approach to promote functional recovery post SCI.^{37,38} In the present study, we demonstrate the function of the UTX/miR-24 epigenetic network in the vascular regeneration of SCI for the very first time (Figure 8D). UTX has been functionally linked to many physical and pathological processes, including embryonic development,^{39,40} tumor progression,^{41–44} inflammation,⁴⁵ and stem cell differentiation^{46,47} by H3K27 demethylation-dependent or -independent gene transcription. Although UTX

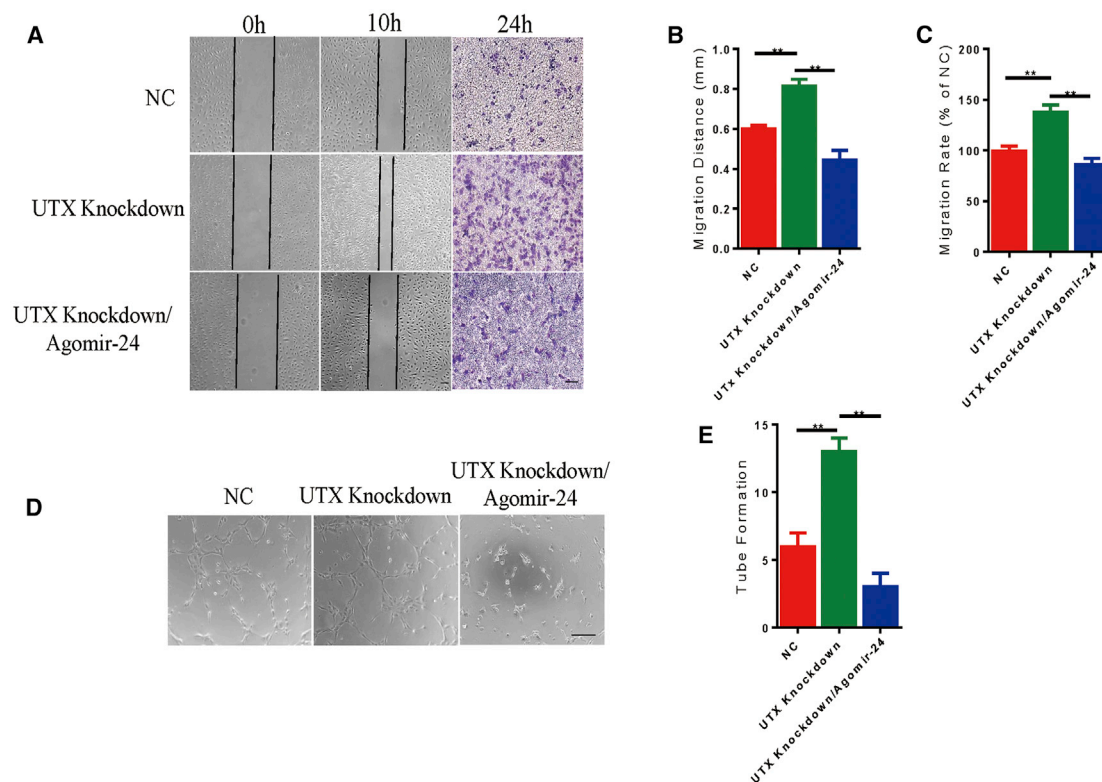


Figure 6. miR-24 Abolished the Effect of UTX Knockdown on Migration and Canalicularization of Endothelial Cells *In Vitro*

(A) Representative images of horizontal migration by wound healing experiment (first and second columns) and vertical migration by Transwell experiment (third column) of HUVECs in the UTX knockdown group, UTX knockdown with miR-24 overexpression group, and control group. Scale bars, 100 μ m. (B and C) Quantification of (A): migration distance (B) and migration rate (C). (D) Representative images of canalicularization of HUVECs in the UTX knockdown group, UTX knockdown with miR-24 overexpression group, and control group. Scale bar, 200 μ m. (E) Quantification of (D). Bars indicate mean \pm SEM; n = 6 per group. **p < 0.01 compared with the control group.

was shown to be required for nuclear factor κ B (NF- κ B)-dependent inflammatory response of ECs,⁴⁸ the regenerative regulation mediated by UTX in SCI is still unclear. We first examined the changes of several key epigenetic regulators post SCI, and we found that the mRNA level of UTX increased significantly post SCI, whereas the changes of other epigenetic factors are variable at different time points post SCI. We further demonstrated the markedly elevated occupancy of UTX in ECs post SCI. These results indicated that UTX may play a critical role in the function of ECs in SCI.

Then, we found that KO of UTX in Tek⁺ ECs can significantly promote vascular regeneration post SCI. Importantly, the KO of UTX in Tek⁺ ECs also promotes the improvement of sensory and locomotive function post SCI. These results indicate that UTX was activated in response to the specific environmental cues post SCI. We previously examined the changes of multiple miRNAs in SCI, among which miR-24 was one of the significantly differentiated expressed miRNAs post SCI.²⁰ Interestingly, we found that modification of UTX can affect the expression level of miR-24 in ECs *in vitro*. miR-24 inhibited the migration and tube formation of ECs as indicated by us and other studies.^{24,49,50} In addition, we showed that agomir-24 significantly abolished the promotive effect of UTX knock-

down on angiogenesis of ECs *in vitro*. Considering that UTX acts as a chromatin regulator to mediate the open of chromatin to enable binding of transcriptional factor and initiate gene transcription, we conducted ChIP assay to reveal that UTX can directly bind to the promoter of miR-24. Moreover, UTX induced the demethylation and initiated the transcription of miR-24 as methylation sequencing assay showed. These data indicate the potential epigenetic network of UTX and miR-24 involved in the regulation of SCI. Further, bioinformatics analysis was performed to predict the potential target genes that might be involved in vascular regeneration in mice and humans. Twenty-one and 24 potential genes were screened out in mice and humans, respectively. Among them, 15 genes are the same for humans and mice, which might be responsible for the downstream mechanism of UTX/miR-24 network post SCI in mice and humans. The treatment targeting UTX may be a potential approach for SCI treatment in mice and humans.

In conclusion, we indicate that UTX deletion can epigenetically promote the vascular regeneration and functional recovery post SCI by forming a regulatory network with miR-24. The present study provides potential therapeutic clues of gene-specific interventions targeting vascular regeneration for the treatment of SCI.

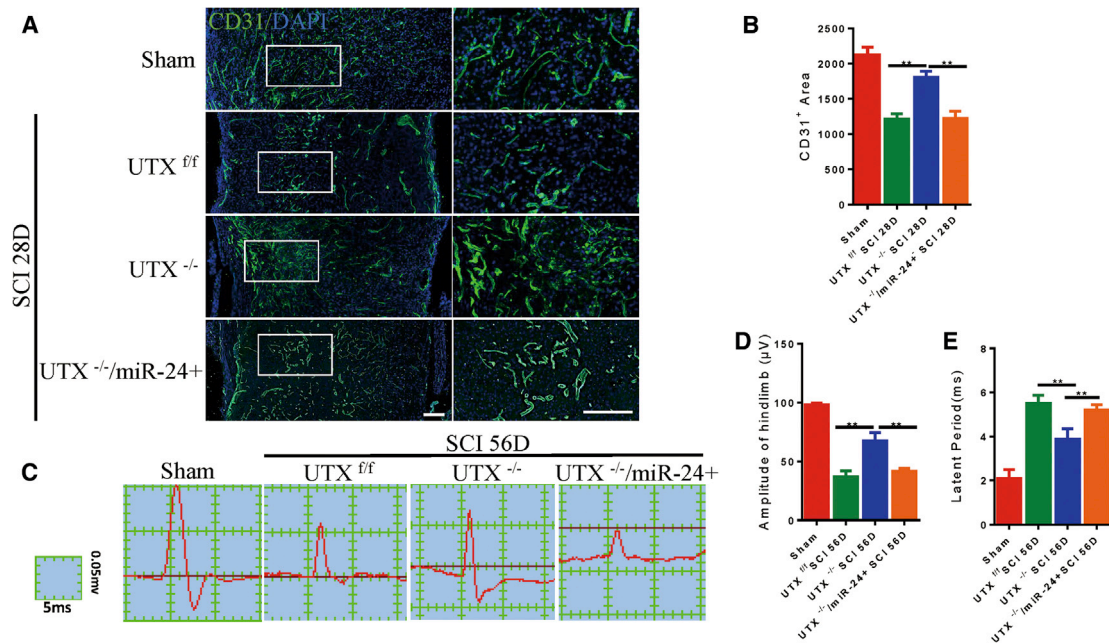


Figure 7. miR-24 Inhibited the Vascular Regeneration in UTX^{-/-} Mice Post SCI

(A) Representative images of immunofluorescent analysis of CD31⁺ (green) blood vessels in mouse spinal cord at 28 days post SCI in sham, UTX^{f/f}, UTX^{-/-}, and UTX^{-/-} mice with miR-24 overexpression. Scale bars, 60 μm. (B) Quantification of (A). (C) Representative images of MEP at 56 days post SCI in UTX^{f/f}, UTX^{-/-}, and UTX^{-/-} mice with miR-24 overexpression. (D) Quantification of the amplitude of MEP in (C). (E) Quantification of the latent period of MEP in (C). Bars indicate mean ± SEM; n = 6 per group. **p < 0.01 compared with the sham group.

MATERIALS AND METHODS

Mice

All animal experimental protocols were approved by the Ethics Committee of Central South University (CSU) for Scientific Research. The animals were kept in specific pathogen-free (SPF) conditions in the Department of Laboratory Animals, CSU. The animals were housed in identical environments (temperature 22°C–24°C; humidity 60%–80%) on a 12-hour light-dark cycle and fed standard rodent chow *ad libitum* with free unlimited food and water. We purchased C57BL/6J (WT) male mice from Charles River. UTX^{flox/flox} (stock no. 021926) mouse strain was purchased from Jackson Laboratory. The Tek-Cre (SJ-008863) mouse strain was purchased from Shanghai Model Organisms. Heterozygous Tek-Cre mice were crossed with UTX^{flox/flox} mice. The offspring were intercrossed to generate the following genotypes: WT, Tek-Cre (mice expressing Cre recombinase driven by Tek promoter), UTX^{flox/flox} (mice homozygous for UTX flox allele, referred to as “UTX^{f/f}” in the text), and Tek-Cre; UTX^{flox/flox} (conditional deletion of UTX in Tek lineage cells, referred to as “UTX^{-/-}” in the text).

Establishment of the Contusion SCI Model and Treatment

We anesthetized the mice at 2 months of age with ketamine and xylazine by intraperitoneal (i.p.) injection. All of the mice were anesthetized before performing thoracic spinal cord contusion injuries. After laminectomy at T10, moderate contusion injury of the spinal cord was induced by a modified Allen’s weight drop apparatus

(10-g weight at a vertical height of 20 mm, 10 g × 20 mm). Mice in the sham group were subjected to laminectomy without contusion. Bladders were manually massaged twice daily until full voluntary or autonomic voiding was obtained, and antibiotic (penicillin sodium; North China Pharmaceutical, Shijiazhuang, China) was administered once daily for 3 days postsurgery.

For the miR-24 treatment, the UTX^{-/-} mice were treated with an intraspinal injection of 2 μL Lentivirus-miR-24 (Shanghai Genechem, Shanghai, China) at rostral and caudal sites 3 mm from the lesion epicenter immediately post SCI in the miR-24 overexpression group. Mice in the UTX^{f/f} group and UTX^{-/-} group received the injection of an equal volume of empty vector for negative control (LV-NC; Shanghai Genechem, Shanghai, China).

Evaluation of the Locomotive Function

The locomotive function of hindlimb was evaluated at 1, 3, 7, 14, 21, 28, and 42 days post SCI using the BMS.⁵¹ Two independent examiners who were familiar with the BMS scores and blinded to the experimental design observed each mouse for 5 min. Then the average scores of each mouse were recorded.

Von Frey Filament Test

Von Frey filament test was performed as previously described⁵² with Semmes-Weinstein monofilaments (Stoetling Company, Dale, IL, USA). In brief, the monofilament was used to stimulate the center

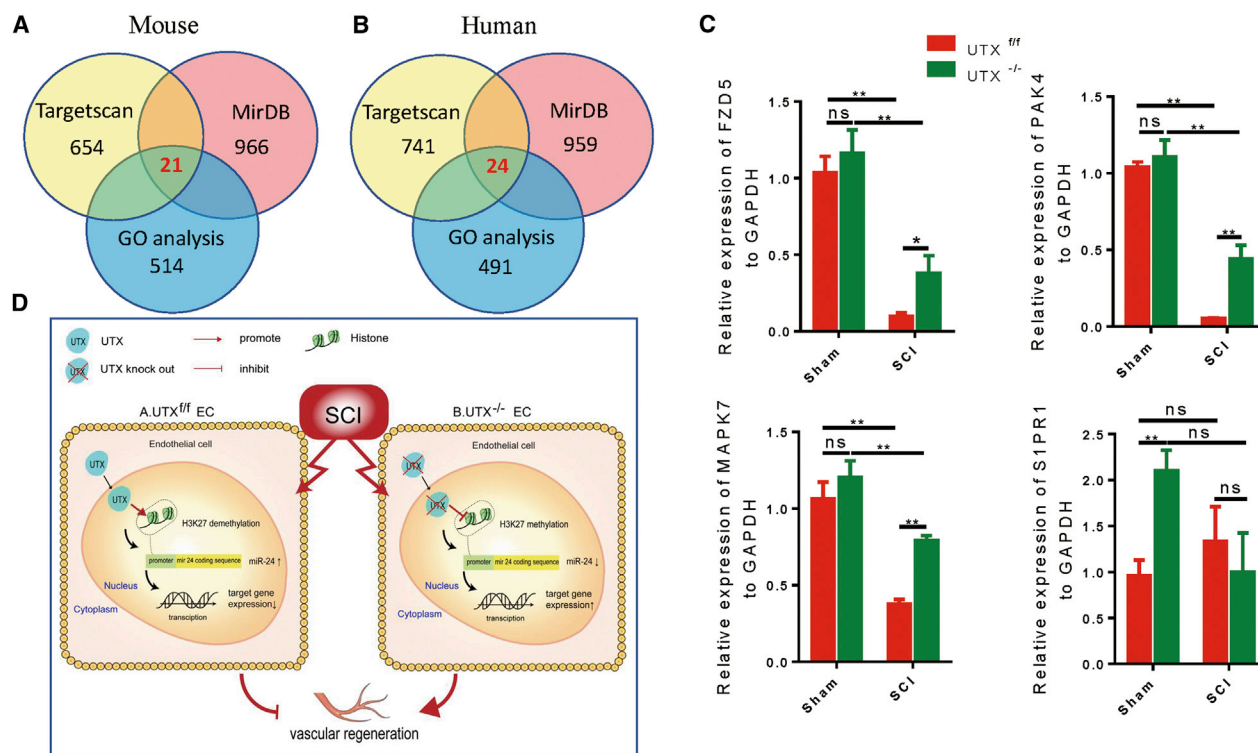


Figure 8. Prediction of miR-24 Target mRNAs Related to Angiogenesis

(A and B) Gene ontology (GO) analysis (<http://amigo.geneontology.org/amigo>) of genes related to angiogenesis, and prediction of miR-24 target mRNA by TargetScan and miRDB in mouse (A) and human (B). (C) The changes of FZD5, PAK4, MAPK7, and S1PR1 at 7 days post SCI in $UTX^{+/+}$ and $UTX^{-/-}$ mice by qRT-PCR. Bars indicate mean \pm SEM; $n = 5$ per group. * $p < 0.05$, ** $p < 0.01$. (D) Graphic illustration of this study. When SCI occurs, expression of UTX increases in endothelial cells to promote the transcription of miR-24, leading to the obstruction of vascular regeneration. Knockout of UTX in endothelial cells benefits the vascular regeneration post SCI. ns, no significance.

of the plantar surface of the hind paw until the filament buckled. The positive response was defined as follows: rapid hind paw withdrawal or sudden hind paw licking. The filament should be smaller/larger in the next trial if the response shows positive/negative. The minimum force that produced a positive response in more than 50% of the trials was determined as the withdrawal threshold. Tests were performed three times with an interval of 10 min before surgery and at 7, 14, 21, 28, and 42 days postsurgery.

Unilateral Hargreaves Thermal Test

The Hargreaves test for thermal hyperalgesia was conducted as previously described.⁵³ In brief, mice were placed on a thin glass pane to acclimate to the testing room for 1 h. The hind paw was stimulated by the specific intensity infrared radiation (Ugo Basile, Comerio, VA, USA). A fiber-optic sensor on the movable infrared heat source was used to measure the withdrawal time. The positive response was defined as follows: rapid hind paw withdrawal or sudden hind paw licking. Tests were performed three times with an interval of 10 min before surgery and at 7, 14, 21, 28, and 42 days postsurgery.

Electrophysiology

The MEPs of hindlimb were recorded as previously described.⁵⁴ After effective anesthesia, stimulating electrodes were placed on the surface

of the skull corresponding to the motor area of the cerebral cortex, and recording electrodes were inserted into the tibialis anterior muscle of the contralateral hindlimb. Subcutaneous tissue between the stimulating and recording electrodes is used to insert the reference electrode. Mean MEP values (including amplitude and latent period) were captured before surgery (baseline) and 56 days postsurgery. Experimental MEP (mV) represented the relative degree of movement recovery for each mouse.

Immunohistochemistry

After being anesthetized with overdose ketamine and xylazine by i.p. injection, adult mice were perfused with normal saline (NS) via the ascending aorta to allow rapid and sufficient draining of blood flow, then with 10% formalin solution for fixation. Spinal cord tissue was sectioned sagittally into 30- μ m-thick serial sections after fixation and dehydration, and stored at -20°C .

The 30th–35th spinal cord sections were chosen and washed in PBS for 15 min, then with 1% PBST (1% Triton X-100 in PBS [pH 7.4]) for 30 min two times. The slices were incubated with blocking solution (5% BSA in 1% PBST) at room temperature for 1 h. Primary antibodies (anti-UTX, 1:1,000 [Millipore]; anti-CD31, 1:100 [R&D]) were incubated at 4°C overnight. The corresponding secondary

antibodies (Abcam, 1:500) were incubated for 1 h at room temperature.

Sample Preparation and 3D Microvascular Imaging Using SR μ CT

The preparation of experimental samples, SR μ CT scanning, and 3D rendering were performed as described previously.^{23,55} In brief, 28 days postsurgery, all UTX^{+/f} mice or UTX^{-/-} mice in the sham group and the SCI group were anesthetized with overdose ketamine and xylazine by i.p. injection. After perfusion with NS and 10% formalin solution, the component contrast agents (Microfil MV-122; Flow Tech, CA, USA) were constantly injected into the circulatory system (2 mL/min at 140 mm Hg for 5 min). Subsequently, the spinal cord segments (approximately 3 mm in length) containing the injury site were harvested and post-fixed in 10% formalin solution for 24 h at 4°C.

SR μ CT scanning was performed at the BL13W1 biomedical beamline in the Shanghai Synchrotron Radiation Facility (SSRF) in China after sample dehydration using a series of graded ethanol. To obtain high X-ray attenuation contrast images, the monochromatic X-ray energy was adjusted to 15 keV, the exposure time was set to 2.5 s, and the sample-to-detector distance was adjusted to 2 cm. A total of 720 initial projection images were captured by the detector (Photonic Science, UK), the effective pixel size of which is 3.25 μ m/pixel. In addition, 12 flat-field images were recorded without sample in the SR beamline path. Five dark-field images were captured when the light source was switched off; they were used to subtract background signal and normalize the image intensity.

After SR μ CT scanning, all of the projection images were reconstructed into digital slice sections using PITRE software (programmed by the BL13W1 experimental station) based on the filtered back-projection (FBP) algorithm. Then, a series of 2D slices was rendered into a 3D presentation using the VG Studio Max 3D reconstruction software (Version 2.1; Volume Graphics, Germany) and Dragonfly Visualization and Analysis Software (Version 4.1; Germany).

To compare the 3D vascular regeneration of the spinal cord in different groups, we selected the regions of interest (ROIs) at the same level of the spinal cord (approximately 3 mm) in each tomography dataset. The vasculature was extracted from the parenchyma based on the iterative gray level-based threshold algorithm.⁵⁶ Then, the vascular morphological parameter can be calculated by the Image Pro Analyzer 3D software (Version 7.0; Media Cybernetics, Rockville, MD, USA).

RNA Isolation and qRT-PCR

The spinal cord tissue for RNA isolation is 1 cm in length, around the injury site. For *in vitro* experiments, 3–5 $\times 10^5$ cells were harvested for RNA isolation. According to the manufacturer's protocol, total RNA was extracted using TRIzol (Invitrogen). Total RNA was prepared by reverse transcription to cDNA using the PrimeScript RT

reagent Kit (Takara), and qRT-PCR was performed using the SYBR Premix Ex Taq (Takara) following the specifications. Primers were designed by RiboBio for the quantitative detection of miRNA expression, and miR-U6 was used as an internal control. For the quantification of mRNA expression, primers were provided by Sangon Biotech (Shanghai, China). The expression of GAPDH was used as an internal control. The analysis of gene expression was performed using the 2^{- $\Delta\Delta$ Ct} method.

Cell Culture and Transfection

The Cancer Research Institute of CSU provided HUVEC lines purchased from the China Cell Culture Center (Shanghai, China).²³ HUVEC lines were thawed and seeded in a six-well plate at 1 $\times 10^5$ cells/well, cultured in conditions of RPMI 1640 (GIBCO) with 10% fetal bovine serum (FBS) and 100 U/mL penicillin supplemented at 37°C with 5% CO₂ in a humidified atmosphere and incubated overnight. Cell lines were transfected with LV-UTX (lentivirus for overexpressing UTX) at an MOI of 1:10 (Shanghai Genechem, Shanghai, China). UTX small interfering RNA (siRNA) or siRNA negative control (50 nM; Shanghai Genechem, Shanghai, China), the agomir-24 (50 nM), antagomir-24 (200 nM), and negative control (200 nM) (Ribo, Guangzhou, China) were used according to the manufacturer's protocol.

Transwell Chamber Migration Assay

We use the Transwell chamber with 8- μ m filter inserts (Corning, Beijing, China) without Matrigel to perform cell migration assay. HUVECs were digested into 100- μ L cell suspensions after trypsin treatment; the upper chamber was filled with 2 $\times 10^5$ cells/mL containing RPMI 1640 medium and 1% BSA, and the lower chamber was filled with 600 μ L RPMI 1640 medium containing 10% FBS. After 24-h treatment, the non-migrated cells on the upper chamber were removed, and the migrated cells on the lower surface were fixed in 100% methanol for 30 min. Subsequently, cells on the lower surface of the membrane were stained with 0.1% crystal violet for 20 min and quantified by counting five random fields. Experiments were repeated six times (n = 6).

Scratch Wound Migration Assay

HUVECs were incubated on six-well plates overnight. The monolayer cells at a confluence rate of 90% were scraped in a cross shape using a 200- μ L pipette tip (at time 0) and photographed with Microscope (CKX41; Olympus Corporation, Tokyo, Japan) to record the wound width; then cells were washed with PBS three times to clean the scratch area and were recovered for 10 h. Images were captured again for migration measurement. The Image-Pro Plus software (Media Cybernetics, Rockville, MD, USA) was used for measuring the distance between the sides of the scratch in five random fields. Experiments were repeated six times (n = 6).

Capillary Network Formation Assay

The assay of capillary network formation was evaluated using the *In Vitro* Angiogenesis Assay Tube Formation Kit (Cultrex, USA) according to the manufacturer's instructions. HUVECs were

trypsinized to suspensions and seeded in 96-well plates pre-coated with 50 μ L Matrigel at 1×10^4 cells/well. After 12 h for network formation, the cells were stained with calcein-AM (2 mM) for 15 min, and images were taken with a fluorescence microscope (Olympus BX51, Japan). Quantitative analysis was performed with the Image-Pro Plus software (Media Cybernetics, Rockville, MD, USA) by counting the network structure in five random fields. Experiments were repeated six times ($n = 6$).

ChIP Assay

The Thermo Fisher ChIP Kit (catalog no. 26156) was used for the assay. We used 1% formaldehyde to crosslink with the crude homogenate from the HUVECs at room temperature for 10 min and then stopped the reaction by adding glycine (0.25 mol/L). Collect the pellet after centrifugation, and lyse cells in SDS lysis buffer containing protease inhibitor cocktail. The lysis was performed with sonicated treatment (30% power, 30 s on and 30 s off for 10 cycles; Diagenode, Denville, NJ, USA) to break DNA into fragments of 200–1,000 bp. Samples were first pre-cleaned by protein G agarose and then subjected to immunoprecipitation overnight with 2 mg of UTX antibodies (1:50; Cell Signaling Technology, Danvers, MA, USA) overnight at 4°C. Use 10%–20% of the sample as an input (a positive control) for immunoprecipitation. After purification, the DNA fragments with the primers for miR-24 promoter were amplified using qRT-PCR.

Western Blot

The expression level of UTX was analyzed by western blot. The protein extraction was centrifuged, and the concentration of supernatants was evaluated by DC protein assay (BioRad Laboratories, Hercules, CA, USA); then the proteins were separated by SDS-PAGE and blotted on a polyvinylidene fluoride membrane (Bio-Rad Laboratories, Hercules, CA, USA). After incubation in specific antibodies, proteins were detected using an enhanced chemiluminescence kit (Amersham Biosciences, Pittsburgh, PA, USA). The target protein concentrations were examined by antibodies recognizing mouse UTX (1:1,000; Cell Signaling Technology, Danvers, MA, USA) and β -Actin (1:1,000; Cell Signaling Technology, Danvers, MA, USA).

DNA Extraction, MSP, and BSP

HUVECs genomic DNA was isolated with the Easypure Genomic DNA kit (TransGen Biotech, Beijing, China). After genomic DNA was isolated, the EZ DNA Methylation-Gold Kit (Zymo Research Corporation, CA, USA) was used for bisulfite conversion and purification according to protocol. Then, methylation-specific PCR (MSP) was performed for methylated and unmethylated forms by simultaneous use of primers. The positive controls in PCRs were performed with HUVECs, and the negative controls were performed with water, respectively. The bisulfite sequencing PCR (BSP) primer was designed by Sangon Biotech (Shanghai). pMD19-T (Takara, Beijing, China) was used for purifying and cloning of amplified PCR products. Five to ten clones of each cell were sequenced. CpG viewer, QUMA, and BIO-analyzer were used for comprehensively and comparatively calculating the percentage of methylation.

In Situ Hybridization

We performed *in situ* hybridization of miR-24 accompanied by CD31 (endothelial marker) immunostaining. Spinal cord cryosections (8 μ m) were dried at room temperature and fixed with 4% paraformaldehyde (PFA; prepared with diethyl pyrocarbonate [DEPC] water) for 10 min; then the sections were washed by PBS (pH 7.4) three times on the shaking bed for 5 min. Samples were digested by proteinase K (20 μ g/mL) for 5 min at 37°C, and then sections were washed three times for 5 min with PBS (prepared with DEPC water). Samples were treated by pre-hybridization buffer for 1 h at 37°C; then we poured out the pre-hybridization buffer and added the miR-24-specific probe (Servicebio Technology, Wuhan, China) overnight at 60°C. The hybrid solution was washed by $2 \times$ saline sodium citrate (SSC) at 37°C for 10 min, $1 \times$ SSC two times at 37°C for 5 min, and $0.5 \times$ SSC for 10 min at room temperature. Next, sections were incubated with blocking solution (5% BSA in 1% PBST) at room temperature for 1 h. Primary antibodies (anti-CD31, 1:100; R&D) were incubated at 4°C overnight. The corresponding secondary antibodies (1:500; Abcam) were incubated for 1 h at room temperature.

Statistical Analysis

All data were presented in the form of means \pm SEM. Unpaired t test was used to compare two groups; paired t test was used to compare pre- and post-treatment values. For the analysis of the differences among three or more groups or between the groups over time, one-way or two-way ANOVA was performed with Tukey's post hoc test. All statistical analyses were carried out using SPSS 19.0 software. $p < 0.05$ was considered statistically significant.

SUPPLEMENTAL INFORMATION

Supplemental Information can be found online at <https://doi.org/10.1016/j.ymthe.2019.08.009>.

AUTHOR CONTRIBUTIONS

J.H. and H.L. designed and supervised the study. S.N., Z.L., and L.J. did the experiments. Z.G., P.L., X.X., and C.L. analyzed data. S.N. and Z.L. wrote the paper. S.N., Z.L., Y.C., C.D., and T.W. scientifically revised the manuscript. All authors contributed to and approved the manuscript.

CONFLICTS OF INTEREST

The authors declare no competing interests.

ACKNOWLEDGMENTS

This work was supported by the National Natural Science Foundation of China (grants 81874004, 81672174, and 81371956), the Science and Technology Commission of Hunan Province of China (grant 2017SK2061), and the Fundamental Research Funds for the Central Universities of Central South University (grants 2016zzts123 and 2016zzts534). The authors would like to thank Prof. Tiqiao Xiao, Prof. Yanan Fu, and other staff at the BL13W1 station of the Shanghai Synchrotron Radiation Facility (SSRF), Shanghai, China; Prof. Hui Xie and other staff from the Movement System Injury and Repair Research Center, Xiangya Hospital, Central South University,

Changsha, China; and Prof. Xianghang Luo and other staff from the Department of Endocrinology, Endocrinology Research Center, Xiangya Hospital of Central South University, Changsha, China, for their kind assistance during the experiments.

REFERENCES

- Kumar, R., Lim, J., Mekary, R.A., Rattani, A., Dewan, M.C., Sharif, S.Y., Osorio-Fonseca, E., and Park, K.B. (2018). Traumatic Spinal Injury: Global Epidemiology and Worldwide Volume. *World Neurosurg.* *113*, e345–e363.
- Figley, S.A., Khosravi, R., Legasto, J.M., Tseng, Y.F., and Fehlings, M.G. (2014). Characterization of vascular disruption and blood-spinal cord barrier permeability following traumatic spinal cord injury. *J. Neurotrauma* *31*, 541–552.
- Ahuja, C.S., Wilson, J.R., Nori, S., Kotter, M.R.N., Druschel, C., Curt, A., and Fehlings, M.G. (2017). Traumatic spinal cord injury. *Nat. Rev. Dis. Primers* *3*, 17018.
- Tran, A.P., Warren, P.M., and Silver, J. (2018). The Biology of Regeneration Failure and Success After Spinal Cord Injury. *Physiol. Rev.* *98*, 881–917.
- Sapieha, P. (2012). Eyeing central neurons in vascular growth and reparative angiogenesis. *Blood* *120*, 2182–2194.
- Ng, M.T., Stammers, A.T., and Kwon, B.K. (2011). Vascular disruption and the role of angiogenic proteins after spinal cord injury. *Transl. Stroke Res.* *2*, 474–491.
- Whetstone, W.D., Hsu, J.Y., Eisenberg, M., Werb, Z., and Noble-Haeusslein, L.J. (2003). Blood-spinal cord barrier after spinal cord injury: relation to revascularization and wound healing. *J. Neurosci.* *74*, 227–239.
- Loscalzo, J., and Handy, D.E. (2014). Epigenetic modifications: basic mechanisms and role in cardiovascular disease (2013 Grover Conference series). *Pulm. Circ.* *4*, 169–174.
- Kundaje, A., Meuleman, W., Ernst, J., Bilenky, M., Yen, A., Heravi-Moussavi, A., Kheradpour, P., Zhang, Z., Wang, J., Ziller, M.J., et al.; Roadmap Epigenomics Consortium (2015). Integrative analysis of 111 reference human epigenomes. *Nature* *518*, 317–330.
- Bauer, A.J., and Martin, K.A. (2017). Coordinating Regulation of Gene Expression in Cardiovascular Disease: Interactions between Chromatin Modifiers and Transcription Factors. *Front. Cardiovasc. Med.* *4*, 19.
- Cloos, P.A., Christensen, J., Agger, K., and Helin, K. (2008). Erasing the methyl mark: histone demethylases at the center of cellular differentiation and disease. *Genes Dev.* *22*, 1115–1140.
- Dreger, H., Ludwig, A., Weller, A., Stangl, V., Baumann, G., Meiners, S., and Stangl, K. (2012). Epigenetic regulation of cell adhesion and communication by enhancer of zeste homolog 2 in human endothelial cells. *Hypertension* *60*, 1176–1183.
- Zhou, V.W., Goren, A., and Bernstein, B.E. (2011). Charting histone modifications and the functional organization of mammalian genomes. *Nat. Rev. Genet.* *12*, 7–18.
- Calo, E., and Wysocka, J. (2013). Modification of enhancer chromatin: what, how, and why? *Mol. Cell* *49*, 825–837.
- Franeau, S., Pali, C.G., Allan, D.S., and Brand, M. (2015). Epigenetic regulation of endothelial-cell-mediated vascular repair. *FEBS J.* *282*, 1605–1629.
- Lee, J.Y., Na, W.H., Choi, H.Y., Lee, K.H., Ju, B.G., and Yune, T.Y. (2016). Jmjd3 mediates blood-spinal cord barrier disruption after spinal cord injury by regulating MMP-3 and MMP-9 expressions. *Neurobiol. Dis.* *95*, 66–81.
- Agger, K., Cloos, P.A., Christensen, J., Pasini, D., Rose, S., Rappsilber, J., Issaeva, I., Canaani, E., Salcini, A.E., and Helin, K. (2007). UTX and JMJD3 are histone H3K27 demethylases involved in HOX gene regulation and development. *Nature* *449*, 731–734.
- Lan, F., Bayliss, P.E., Rinn, J.L., Whetstone, J.R., Wang, J.K., Chen, S., Iwase, S., Alpatov, R., Issaeva, I., Canaani, E., et al. (2007). A histone H3 lysine 27 demethylase regulates animal posterior development. *Nature* *449*, 689–694.
- Ouyang, Y.B., Xu, L., Yue, S., Liu, S., and Giffard, R.G. (2014). Neuroprotection by astrocytes in brain ischemia: importance of microRNAs. *Neurosci. Lett.* *565*, 53–58.
- Hu, J.Z., Huang, J.H., Zeng, L., Wang, G., Cao, M., and Lu, H.B. (2013). Anti-apoptotic effect of microRNA-21 after contusion spinal cord injury in rats. *J. Neurotrauma* *30*, 1349–1360.
- Wang, S., Aurora, A.B., Johnson, B.A., Qi, X., McAnally, J., Hill, J.A., Richardson, J.A., Bassel-Duby, R., and Olson, E.N. (2008). The endothelial-specific microRNA miR-126 governs vascular integrity and angiogenesis. *Dev. Cell* *15*, 261–271.
- Poliseno, L., Tuccillo, A., Mariani, L., Evangelista, M., Citti, L., Woods, K., Mercatanti, A., Hammond, S., and Rainaldi, G. (2006). MicroRNAs modulate the angiogenic properties of HUVECs. *Blood* *108*, 3068–3071.
- Hu, J., Ni, S., Cao, Y., Zhang, T., Wu, T., Yin, X., Lang, Y., and Lu, H. (2016). The Angiogenic Effect of microRNA-21 Targeting TIMP3 through the Regulation of MMP2 and MMP9. *PLoS ONE* *11*, e0149537.
- Fiedler, J., Jazbutyte, V., Kirchmaier, B.C., Gupta, S.K., Lorenzen, J., Hartmann, D., Galuppo, P., Kneitz, S., Pena, J.T., Sohn-Lee, C., et al. (2011). MicroRNA-24 regulates vascularly after myocardial infarction. *Circulation* *124*, 720–730.
- Zhou, Q., Gallagher, R., Ufret-Vincenty, R., Li, X., Olson, E.N., and Wang, S. (2011). Regulation of angiogenesis and choroidal neovascularization by members of microRNA-23~27~24 clusters. *Proc. Natl. Acad. Sci. USA* *108*, 8287–8292.
- Lan, F., Pan, Q., Yu, H., and Yue, X. (2015). Sulforaphane enhances temozolomide-induced apoptosis because of down-regulation of miR-21 via Wnt/ β -catenin signaling in glioblastoma. *J. Neurochem.* *134*, 811–818.
- Ma, X., Conklin, D.J., Li, F., Dai, Z., Hua, X., Li, Y., Xu-Monette, Z.Y., Young, K.H., Xiong, W., Wysoczynski, M., et al. (2015). The oncogenic microRNA miR-21 promotes regulated necrosis in mice. *Nat. Commun.* *6*, 7151.
- Listing, H., Mardin, W.A., Wohlfromm, S., Mees, S.T., and Haier, J. (2015). MiR-23a/-24-induced gene silencing results in mesothelial cell integration of pancreatic cancer. *Br. J. Cancer* *112*, 131–139.
- Zhou, N., and Yan, H.L. (2018). MiR-24 promotes the proliferation and apoptosis of lung carcinoma via targeting MAPK7. *Eur. Rev. Med. Pharmacol. Sci.* *22*, 6845–6852.
- Lorenzen, J.M., Kaucsar, T., Schauer, C., Schmitt, R., Rong, S., Hübner, A., Scherf, K., Fiedler, J., Martino, F., Kumarswamy, R., et al. (2014). MicroRNA-24 antagonism prevents renal ischemia reperfusion injury. *J. Am. Soc. Nephrol.* *25*, 2717–2729.
- Rodrigues, L.F., Moura-Neto, V., and de Sampaio e Spohr, T.C.L. (2018). Biomarkers in Spinal Cord Injury: from Prognosis to Treatment. *Mol. Neurobiol.* *55*, 6436–6448.
- Meng, Q., Zhuang, Y., Ying, Z., Agrawal, R., Yang, X., and Gomez-Pinilla, F. (2017). Traumatic Brain Injury Induces Genome-Wide Transcriptomic, Methylation, and Network Perturbations in Brain and Blood Predicting Neurological Disorders. *EBioMedicine* *16*, 184–194.
- Iadecola, C. (2017). The Neurovascular Unit Coming of Age: A Journey through Neurovascular Coupling in Health and Disease. *Neuron* *96*, 17–42.
- Lok, J., Gupta, P., Guo, S., Kim, W.J., Whalen, M.J., van Leyen, K., and Lo, E.H. (2007). Cell-cell signaling in the neurovascular unit. *Neurochem. Res.* *32*, 2032–2045.
- del Zoppo, G.J. (2009). Inflammation and the neurovascular unit in the setting of focal cerebral ischemia. *Neuroscience* *158*, 972–982.
- Xing, C., Hayakawa, K., Lok, J., Arai, K., and Lo, E.H. (2012). Injury and repair in the neurovascular unit. *Neurol. Res.* *34*, 325–330.
- Cao, Y., Wu, T.D., Wu, H., Lang, Y., Li, D.Z., Ni, S.F., Lu, H.B., and Hu, J.Z. (2017). Synchrotron radiation micro-CT as a novel tool to evaluate the effect of agomir-210 in a rat spinal cord injury model. *Brain Res.* *1655*, 55–65.
- Hu, J., Zeng, L., Huang, J., Wang, G., and Lu, H. (2015). miR-126 promotes angiogenesis and attenuates inflammation after contusion spinal cord injury in rats. *Brain Res.* *1608*, 191–202.
- Welstead, G.G., Creighton, M.P., Bilodeau, S., Cheng, A.W., Markoulaki, S., Young, R.A., and Jaenisch, R. (2012). X-linked H3K27me3 demethylase Utx is required for embryonic development in a sex-specific manner. *Proc. Natl. Acad. Sci. USA* *109*, 13004–13009.
- Lee, S., Lee, J.W., and Lee, S.K. (2012). UTX, a histone H3-lysine 27 demethylase, acts as a critical switch to activate the cardiac developmental program. *Dev. Cell* *22*, 25–37.
- Schulz, W.A., Lang, A., Koch, J., and Greife, A. (2019). The histone demethylase UTX/KDM6A in cancer: Progress and puzzles. *Int. J. Cancer* *145*, 614–620.
- Research Watch (2018). KDM6A Loss Induces Aggressive Pancreatic Cancer in Mice. *Cancer Discov.* *8*, 528.

43. Ezponda, T., Dupéré-Richer, D., Will, C.M., Small, E.C., Varghese, N., Patel, T., Nabet, B., Popovic, R., Oyer, J., Bulic, M., et al. (2017). UTX/KDM6A Loss Enhances the Malignant Phenotype of Multiple Myeloma and Sensitizes Cells to EZH2 inhibition. *Cell Rep.* *21*, 628–640.
44. Andricovich, J., Perkail, S., Kai, Y., Casasanta, N., Peng, W., and Tzatsos, A. (2018). Loss of KDM6A Activates Super-Enhancers to Induce Gender-Specific Squamous-like Pancreatic Cancer and Confers Sensitivity to BET Inhibitors. *Cancer Cell* *33*, 512–526.e8.
45. Li, X., Zhang, Q., Shi, Q., Liu, Y., Zhao, K., Shen, Q., Shi, Y., Liu, X., Wang, C., Li, N., et al. (2017). Demethylase Kdm6a epigenetically promotes IL-6 and IFN- β production in macrophages. *J. Autoimmun.* *80*, 85–94.
46. Hemming, S., Cakouros, D., Isenmann, S., Cooper, L., Menicanin, D., Zannettino, A., and Gronthos, S. (2014). EZH2 and KDM6A act as an epigenetic switch to regulate mesenchymal stem cell lineage specification. *Stem Cells* *32*, 802–815.
47. Thieme, S., Gyárfás, T., Richter, C., Özhan, G., Fu, J., Alexopoulou, D., Muders, M.H., Michalk, I., Jakob, C., Dahl, A., et al. (2013). The histone demethylase UTX regulates stem cell migration and hematopoiesis. *Blood* *121*, 2462–2473.
48. Yoshiki Higashijima, Y.M.T.S., Yohei Abe, V.M.L.M., Toshihiro Tanaka, A.T.M.M., Hiroshi Kimura, T.F.H.A., and Glass, Y.K. (2018). Coordinated demethylation of H3K9 and H3K27 is required for rapid inflammatory responses of endothelial cells. *bioRxiv*. <https://doi.org/10.1101/456491>.
49. Zheng, Y., Li, Y., Liu, G., Qi, X., and Cao, X. (2018). MicroRNA-24 inhibits the proliferation and migration of endothelial cells in patients with atherosclerosis by targeting importin- $\alpha 3$ and regulating inflammatory responses. *Exp. Ther. Med.* *15*, 338–344.
50. Meloni, M., Marchetti, M., Garner, K., Littlejohns, B., Sala-Newby, G., Xenophontos, N., Floris, I., Suleiman, M.S., Madeddu, P., Caporali, A., and Emanuelli, C. (2013). Local inhibition of microRNA-24 improves reparative angiogenesis and left ventricle remodeling and function in mice with myocardial infarction. *Mol. Ther.* *21*, 1390–1402.
51. Basso, D.M., Fisher, L.C., Anderson, A.J., Jakeman, L.B., McTigue, D.M., and Popovich, P.G. (2006). Basso Mouse Scale for locomotion detects differences in recovery after spinal cord injury in five common mouse strains. *J. Neurotrauma* *23*, 635–659.
52. Chaplan, S.R., Bach, F.W., Pogrel, J.W., Chung, J.M., and Yaksh, T.L. (1994). Quantitative assessment of tactile allodynia in the rat paw. *J. Neurosci. Methods* *53*, 55–63.
53. Russell, F.A., Fernandes, E.S., Courade, J.P., Keeble, J.E., and Brain, S.D. (2009). Tumour necrosis factor alpha mediates transient receptor potential vanilloid 1-dependent bilateral thermal hyperalgesia with distinct peripheral roles of interleukin-1beta, protein kinase C and cyclooxygenase-2 signalling. *Pain* *142*, 264–274.
54. Schlag, M.G., Hopf, R., and Redl, H. (2001). Serial recording of sensory, corticomotor, and brainstem-derived motor evoked potentials in the rat. *Somatosens. Mot. Res.* *18*, 106–116.
55. Cao, Y., Wu, T., Yuan, Z., Li, D., Ni, S., Hu, J., and Lu, H. (2015). Three-dimensional imaging of microvasculature in the rat spinal cord following injury. *Sci. Rep.* *5*, 12643.
56. Reichold, J., Stampanoni, M., Lena Keller, A., Buck, A., Jenny, P., and Weber, B. (2009). Vascular graph model to simulate the cerebral blood flow in realistic vascular networks. *J. Cereb. Blood Flow Metab.* *29*, 1429–1443.